Preprints (www.preprints.org) | NOT PEER-REVIEWED | Posted: 5 August 2020 doi:10.20944/preprints202008.0098.v2

On the Construction of Raindrop Erosion Maps for Steel

J. A. Sloan, M. M. Stack

Department of Mechanical and Aerospace Engineering,

University of Strathclyde, Glasgow UK

Graphical Abstract:

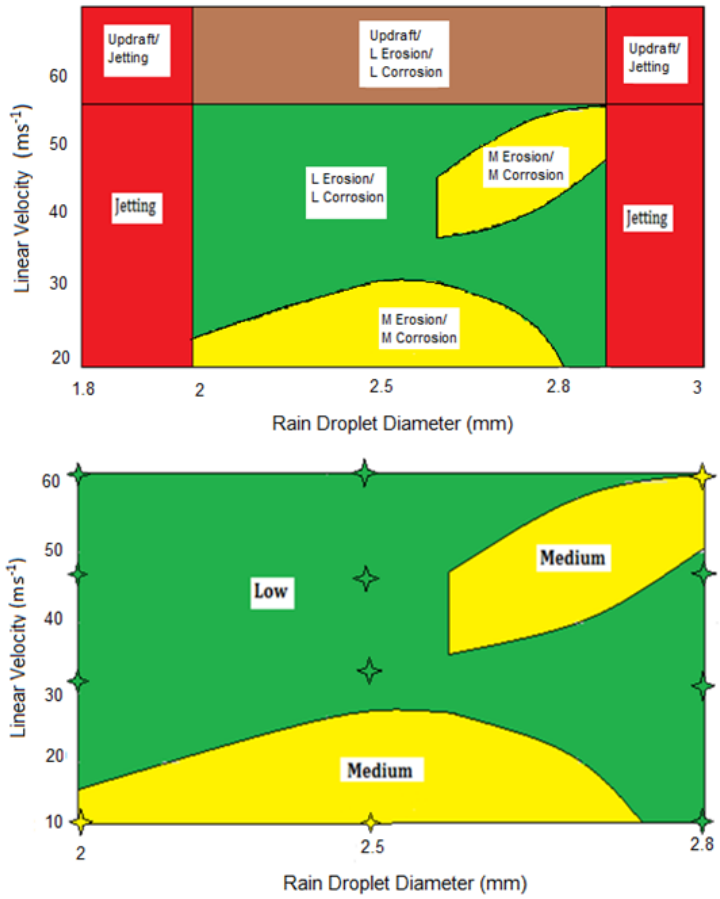

Raindrop erosion damage greatly varies with velocity, particle size and target material. Tests were conducted on carbon steel over a range of impact velocity and raindrop sizes. Using the carbon steel test results as a reference, mechanistic and wastage erosion maps are created. These Erosion mapping techniques can be used for the identification, classification and prediction of material degradation.

Preprints (www.preprints.org) | NOT PEER-REVIEWED | Posted: 5 August 2020 doi:10.20944/preprints202008.0098.v2

Acronyms

AFP	Automated fibre placement
ATL	Automated tape layup
CFRP	Carbon fibre reinforcement plastic
EDS	Energy dispersive spectroscopy
EWEA	European wind energy association
GFRP	Glass fibre reinforcement plastic
GW	Giga Watts
mm	Millimeters
ml	Milliliters
mg	Milligrams
NDI	Non-destructive inspection
RETR	Rain erosion test rig
SEM	Scanning electron microscopy
UDRI	University of Dayton Research Institute
UK	United Kingdom
WARER	Whirling arm rain erosion rig

Nomenclature

C_l	Speed of sound in liquid (ms^{-1})
C_s	Speed of sound in solid (ms^{-1})
C_ρ	Speed of sound in undistributed density (ms^{-1})
d	Rain droplet diameter (mm)
F	Impact force (N)
m	Mass of raindrop (kg)
ρ_l	Density of liquid (kg/m^3)
ρ_o	Undistributed density of the fluid (kg/m^3)
ρ_s	Density of solid (kg/m^3)
V	Impact velocity (ms^{-1})
V_0	Impact velocity (ms^{-1})

Abstract

Raindrop erosion is a significant materials limiting issue. It can affect materials for transportation and renewable energy converters such as wind turbines as well as all external structures used in the construction industries. In such cases, the raindrop effects can occur over a wide range of impact velocities and particles sizes.

In understanding tribological variable effects, it is useful to study using reference materials. This is because the reference material is well characterized, from previous knowledge of the tribological and corrosion patterns. Further, the well-established chemical composition and stochiometry of the corrosion products provide some background understanding of how effectively, during tribological action, the surface scale adheres to the substrate.

In this study, a carbon steel was used as a reference to study the effects of velocity and drop diameter in a whirling arm erosion test rig. The results were used to establish the conditions where corrosion was accelerated and the environments where aerodynamic effects may have resulted in droplets being deflected the surfaces. Erosion maps were generated to illustrate such mechanisms based on the results.

1. Introduction

Society today aims towards a future where renewable energy resources dominate over productions from fossil fuels and nuclear fission power resources. With weather patterns changing across the globe, speculations of global warming being the major contributor has led the UK government to develop new legislation to meet a cleaner means of power production. Several Energy White Papers, for example that published in 2003, concluded that if the UK is to achieve a reduction in carbon emissions of the required scale then renewable energy will need to contribute at least 30-40% of our electricity generation. [1]

The UK is one of the optimum locations in the world for wind power. By way of illustration of the vast rate of growth in renewable energies, the UK electricity generated by renewable energy increased to over 30% 2019 alone. [2] To accomplish these targets in renewable energies, large investments have been made to improve the efficiencies and overall power contributions from all renewable energy resources. These targets have thus led to an increase in wind turbine numbers and technological advance in the wind energy sector.[3]

Developing wind turbines and improving the efficiency is a very complex procedure with many environmental and tribological factors to take into consideration. Extreme winds and gales cause bending and cyclic loading on the frame and blades of the wind turbine. Abundant rain and hailstone showers affect the aerodynamic efficiency of the blades due to leading edge erosion. As every continent in the world has different environmental conditions, factors such as extreme temperatures, snow/icing and ultra violet light exposure must be brought into consideration when developing these turbines. Off-shore wind farms may have more issues in the long term due to high maintenance costs and the generally large blade lengths in such conditions. This brings a disadvantage of greater wind tip velocities on the blade that accelerates erosion of the leading edge and rapidly decreases the aerodynamic efficiency.

Historically there has been less attention given to the effects of liquid impacts and Field (1999) states it was not until steam turbine blades were found to erode that sparked interest in this subject. [4]. Research in this field became more popular over the decades, as aircraft was getting faster more research was focused on the erosion of aircraft wings. Much research has been focused on the dynamics behind the rain drop impact explaining how damage on the blades occur.

Liquid impacts consist of two main stages, firstly the liquid behaves in a compressible manner generating the so called water hammer pressure. Water hammer pressure is a pressure surge or wave created when a fluid collides with a surface causing it to stop abruptly. These high pressures cause the greatest damage on the surface due to liquid impacts and are maintained while the edge of the contact area between the impacting liquid and the solid moves supersonically with respect to the shock speed.[5]. The interaction of these waves are very complex, depending upon the impact conditions and material properties of the impact surface. A Rayleigh wave is created on impact and travels along the solid surface. The compressed liquid wave in the droplet after a short time duration after impact, extends towards and past the contact periphery between the droplet and the surface. After this point lateral jetting or more commonly known splashing of the droplet occurs. [1]

The water hammer pressure mentioned previously can be calculated using the equations below; [4]

$P = \rho_o c_o V_o$ - *Equation 1*

$$P = \frac{V\rho_l c_l \rho_s c_s}{\rho_l c_l + \rho_s c_s} \text{ - Equation 2}$$

(*Equation 1*) is a simple representation of the water hammer pressure and was originally used to calculate water hammer pressures present in piping systems, based on quite straight forward assumptions. Dear and Field proposed a modified water hammer equation which takes into consideration not only the pressure through the liquid but also the colliding surface. [5]The subscripts in (*Equation 2*) (l) and (s) refer to liquid and solid bodies respectively. An instantaneous approximation of the impact force created by the rain droplet on the surface can be calculated from (*Equation 3*) stated below;

$$F = \frac{mV^2}{d} \text{ - Equation 3}$$

A single rain drop has very little effect on a solid surface; it is the repetitive impacts from rainfall over long periods that cause permanent damage. When the rain drop makes initial contact with the surface, the water hammer pressure produced causes small cavities to gradually form. These cavities were proven to be caused by the formation of pressure waves. Further impacts deepen these cavities before giving rise to stress concentrations in the material that cause more of the material to be removed. The erosion process causes work hardening and further crack growth which leads to greater loss of surface material. [6]. A more recent researcher Hattori (2010) proposed that the fracture toughness and fatigue crack removal was the main mechanism involved in the erosion process. [7]

Damage on wind turbine blades is known as leading edge erosion in the wind industry and can be explained as pitting and gouging around the edge of the blade. Damage of the composite on the leading edge can reduce the aerodynamic efficiency after only two years in service. [8] In an attempt to address this issue of leading edge erosion, companies are researching and developing new materials for protecting the leading edge. Applying elastomeric materials such as tapes to the blades are becoming very effective methods of improving the blades resistance to erosion.

In heavy rainfall impact velocities reach up to 100ms^{-1}, previous work quotes a single rain drop can impact pressures of 140MPa on a surface, with repetitive bombardment these impacts can cause a lot of damage. A 20% reduction in annual energy output due to this phenomenon has been estimated. [9] This highlights the engineering challenge behind reducing this leading edge erosion. In relation to the leading edge erosion, the free fall velocity of a raindrop will have an impact on the overall collision velocity. Keegan et al. [5] shows the free fall velocity only has a minor role in the magnitude of the impact velocity when compared to blade tip velocities. It is possible, through vector calculations to establish an approximation for the impact velocity for a given rain and turbine conditions, through a whole rotor sweep. The maximum impact velocity occurs at 270° on the rotor sweep and is the resultant of the free fall velocity and the tip speed of the blade.

Raindrop diameters vary with respect to climate conditions under which they are formed and conditions of transport in the air. Typical raindrop diameters are commonly in the range between 0.5mm and 5mm, above this maximum diameter droplets are very unstable and begin to fragment.

Kubilay et al. [10]produced a graph for the probability density for the raindrop diameters using the equations derived by Best, [10, 11]as shown in Figure 1.

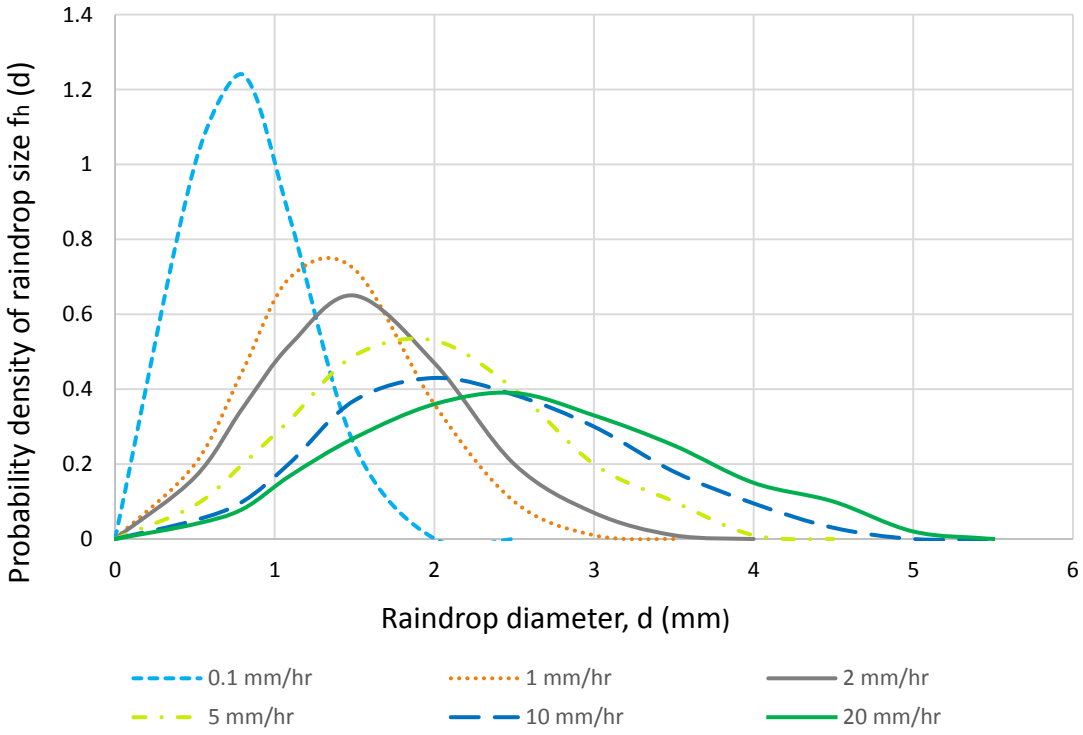

***Figure 1**: Probability density of raindrop size. Calculated using equation from* [1]

As can be observed in the probability graph above, Fig. 1, the average rain droplet diameters during moderately calm rain fall range between 0.5mm and 3mm. The peak or most common raindrop diameters in all variations of rain conditions tested and recorded in the graph, range between 1.4mm and 3mm respectively, ignoring the 0.1mm/h rainfall.

In the present study, the erosion is evaluated over a range of velocities and particle sizes. Morphological study of the damage surfaces is carried out. Based on such observations and mass loss data, erosion maps are constructed based on the results.

Preprints (www.preprints.org) | NOT PEER-REVIEWED | Posted: 5 August 2020 doi:10.20944/preprints202008.0098.v2

2. Experimental Details

2.1 Initial rain erosion test rig apparatus

The original apparatus for the rain erosion test rig (RETR) rig uses horizontal arms on which test specimens are attached and made to rotate in an enclosed chamber under wind turbine simulated conditions (*Figure 2*). The velocity and rain droplet diameters are varied to simulate different rain conditions.

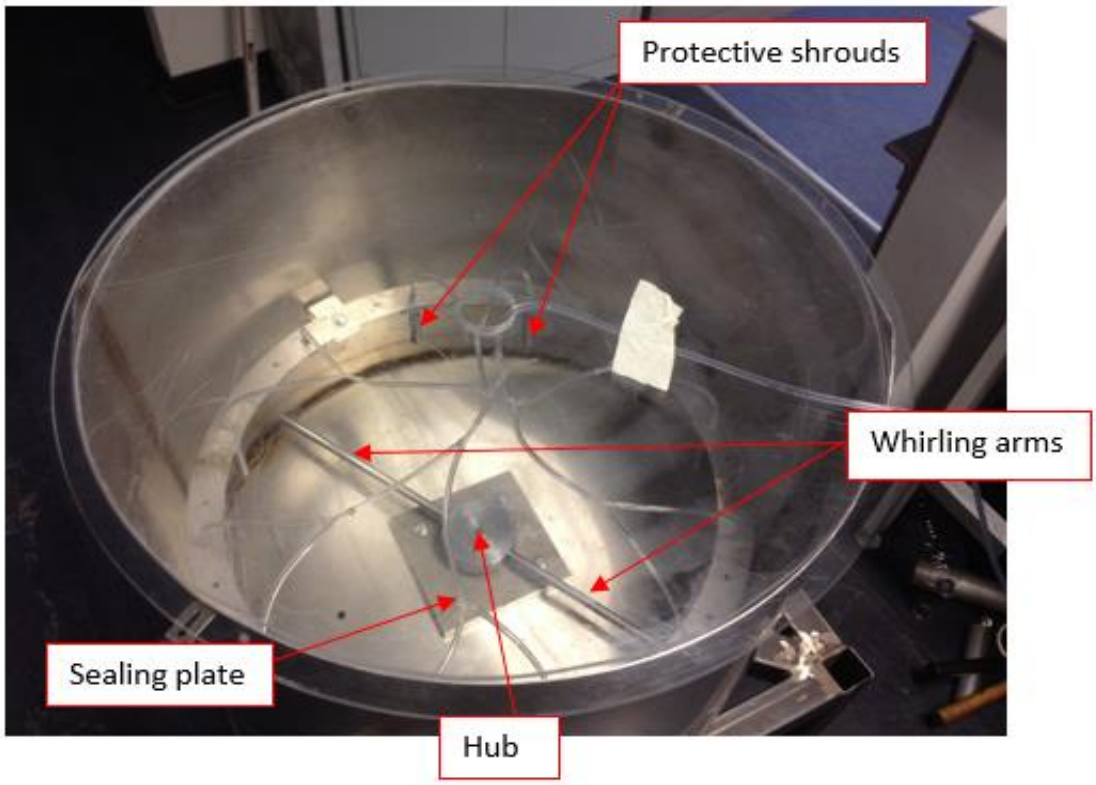

***Figure 2**: Rain erosion test rig after developments*

Powered by an AC motor, a pulley and belt system provides the rotational motion to the hub on which the whirling arms and mounts are connected. The rotational velocity is controlled safely by an AC invertor. A relationship between the rotational velocity of the motor drive shaft and the output frequency of the inverter provides an easy method of controlling the rotational velocity.

Developments were undertaken to increase the rotational velocity of the (RETR). During developments however severe corrosion damage on the bearings resulted in the drive shaft to twist. The damaged caused a distinct wobble on the hub redeeming it too unstable for increasing the rotational velocity before repairs were completed.

A 200CM series peristaltic pump, with a flow rate ranging between 10mL/min and 40mL/min was used to control the flow of water to the needles. This type of pump is an accurate method for

controlling the flow rate, depending on the test conditions. A flow rate equivalent to 25.4mmh^{-1} of rain is widely used by researchers as the worst case scenario of extremely heavy rain fall common in tropical regions.

The needle gauge evaluation was as follows:

$$V_s = \frac{4}{3}\pi r^3 \quad \text{- Equation 4}$$

$$A = \pi(r_o)^2 - \pi(r_i)^2 \quad \text{- Equation 5}$$

$$V_r = A\ x\ 0.0254 \quad \text{- Equation 6}$$

$$N_r = \frac{V_r}{V_s} \quad \text{- Equation 7}$$

The volume of water required for the test was calculated assuming the average raindrop is 2mm in diameter and spherical in shape. (*Equation 4*) gives a volume of the raindrop to be 4.19 x 10^{-9} m^3. The test specimens during these tests had the same diameter of 30mm used in previous work. The hub and whirling arms produce a rotating radius of 0.3015m. The revolving path of the test specimens will then have an outer rotating radius of 0.3155m and an inner radius of 0.2855m which gives an annular area of 0.0566 m^2 according to (*Equation 5*).

As the desired rain fall rate for the tests are to be 25.4mmh^{-1}, the required rainfall volume for one hour is 1.44 x 10^{-3} m^{3}h^{-1} and was calculated using (*Equation 6*). With an average rain drop volume of 4.19 x 10^{-9} m^3 and the rain fall volume over one hour 1.44x10^{-3} m^3 from (*Equation 7*), 343,675 raindrops will be produced per hour and 95 raindrops per second were required.

Referring to section (1.5) the most abundant raindrop diameters for all rainfall conditions ranged between 1.4mm and 3.0mm. For this reason testing in this project focused on raindrop diameters between 1.8mm and 3.0mm, shown in (*Table 1*), which displays the various needle gauges used and the corresponding raindrop diameters they produce.

***Table 1**: Variation of raindrop diameter with needle gauge*

Needle gauge	Needle colour	Raindrop size (mm)
19	White	3.0
21	Green	2.8

Preprints (www.preprints.org) | NOT PEER-REVIEWED | Posted: 5 August 2020 doi:10.20944/preprints202008.0098.v2

23	Blue	2.5
25	Orange	2.0
30	Yellow	1.8

2.2 Test Specimen Holder

Initially a wear resistant adhesive was used to attach the test specimen onto the mount. At the end of the test a new specimen had to replace the existing one so a comparison could be made under different test conditions. Many methods were attempted to remove the specimen from the mount, examples being heat treatment and the development of a jig, which was an attempt at removing the test specimen by force. Both methods were unsuccessful and kept destroying the mounts and damaging the test sample. For this reason, previous testing resulted in a new mount being used for each test.

***Figure 3**: a) Test specimen holder design No. 1 b) Test specimen holder design No. 2*

New designs of the test specimen holder were created and tested. The new design was developed to run tests quicker and more efficiently. Removing samples at the end of testing allowed a comparison of the corrosion and wear scars for various different test conditions. Figure 3 shows the two final designs that were sent to the workshop for construction. Design number 1 demonstrated the most potential with a strong connection due to three small screws. Designs had to be made to produce minimal wear on the test specimens as any mass loss would affect the final results of the tests; for this reason, design 1 was used as the mount during this project.

2.3 Initial testing

$$V = \omega \, x \, r \, x \, \frac{2\pi}{60} \; - \; Equation\ 8$$

Initial tests were carried out on the rig before starting preliminary testing using raindrop impacts, as some major developments were undertaken. The tests were used to confirm the rotational velocity of the rig was the same as before developments. The rotational velocity of the whirling arms for a given frequency from the AC invertor to the motor was measured using an optical tachometer, results are displayed in (*Table 2*). The linear velocity of the test specimen was calculated using (*Equation 8*). The velocities of the rig are seen to be slightly lower than before developments. Reason being the sealing plate rubs against the drive shaft causing a small frictional torque.

***Table 2**: Velocities measured before and after development*

Frequency (Hz)	Average rotational velocity (rad/s)	Linear Velocity (m/s)	Linear velocity of initial rig design (m/s)
10	517.6	16.3	17
20	1044	32.9	35
30	1516	47.7	51
40	1922	60.5	66
50	2197	69.1	78

2.4 SEM and EDS Analysis

Specimens were analysed before and after testing by SEM allowing high resolution images of their topography. Analysis of the images will show whether erosion has taken place. An elemental analysis using EDS was also carried out on the mild steel specimens to indicate the elemental compositions on the surface of the specimen before and after testing. The results display a percentage of each element to determine any oxides or indication of a corrosive process.

2.5 Impact Testing

2.5.1 Mild Steel Specimens

Mild steel is being used as a reference material to calibrate the rig to working conditions that can erode GFRP and CFRP composite materials. The rig was modified to run at faster velocities to produce larger impact energies that will erode the surface of the composites. Initially test specimens

were made from 2mm thick mild steel with a circular diameter of 30mm. In-light of the new mount the test specimens were altered to have a thickness of 5mm, with three M3 holes drilled at 120 degree intervals, 3mm deep, on the bottom surface of the test specimen. An image of the test samples and mount can be observed in Figure 3[a].

3. Results

3.1 Preliminary Testing of Mild Steel

Preliminary testing was carried out to verify the new developments had not affected the rig as a rain erosion test rig. Testing was carried out using gauge 23 needles to produce a 2.5mm diameter raindrop at a wind velocity of 32.9ms^{-1}. Both the mount and test specimen were weighed together before and after the test. The initial testing phase showed a large variation in mass loss and also mass gain in the range of 15mg per 20 minute interval. Between the surfaces of the test specimen and mount was a large build-up of corrosive matter, perhaps caused by the velocity of the whirling arms pulling water and mass particles along the surface of the test specimen and into the gap cavity. There is also a smaller effect from galvanic coupling between the two metals which could be detrimental to the increase in corrosion.

1. The updraft caused from the increasing velocity of the whirling arms affected the trajectory of the rain droplets. Water droplets were seen collecting at the side of the rig walls at faster velocities whereas at lower velocities this was not observed. This indicates that many droplets may not be coming into contact with the test material.

Corrosion between the surfaces denotes other reactions are occurring rather than solely on the top surface of the sample being examined. To improve the accuracy of the results, this variable had to be removed, accomplished by the use of a non-corrosive coating. A thin layer of varnish covered the mounts and the underside of the test specimens where these unwanted reactions were taking place.

Having completed varnishing on the mount and underside of the test specimen, further observations were made.

1. There was still a large unexplained increase in mass
2. Varnish successfully removed any sign of corrosion from in between the test specimen.

Having separated the test specimen from the mount small water droplets were discovered on the varnish in-between the surfaces explaining the unusual variations in mass loss and gain. Further tests were carried out wearing gloves at all times when handling the test specimens. The test specimens were cleaned with acetone at the beginning of each test to remove dust particles from the lab or oil residue from machining. For each weighing the specimen was dismantled from the mount and dried to remove the water on the inner surface. The test subject was then weighed 3 times and an average mass was taken to get the most accurate result possible, as the scales were not in pristine condition. Once most of the variables were eliminated, tests started displaying consistent mass losses.

Preprints (www.preprints.org) | NOT PEER-REVIEWED | Posted: 5 August 2020 doi:10.20944/preprints202008.0098.v2

3.2 Erosion of mild steel with varying linear velocity

Tests were undertaken to study the effect varying the shaft linear velocity has on the mass loss of mild steel. The results show a gradual mass loss as the linear velocity increases, tabulated in Table 4 and discussed in section 4.2.

***Table 4**: Mass loss due to varying linear velocity*

Test duration (minutes)	Invertor setting (Hz)	Shaft linear velocity (m/s)	Total mass loss of subject 1 (mg)	Total mass loss of subject 2 (mg)
0	0	0	0	0
20	10	16.3	0.5	0.3
40	20	32.9	0.6	0.4
60	30	47.7	1	0.7
80	40	60.5	1.1	0.9

3.3 Erosion of steel specimens with changing diameter

The mass loss was taken using a set of weighing scales able to measure to an accuracy of 0.1mg. Results for varying rain droplet diameters at the required velocities are displayed in Tables 5, 6, 7 and 8 respectively. Due to jets of water forming from the end of the needles and producing an inconstancy of raindrops; impact testing on rain drop diameters 1.8mm and 3.0mm could not be undertaken, as specified in section 5.4.

Results show tests at 16.3ms^{-1} encountered the largest mass loss. According to previous work these results display some unusal findings, although more conditions were tested in the present study [14]. Graphs in Figures 11, 12, 13 and 14 in (*section 4.3*) respectively explain the results of varying rain drop diameter in more detail. Observations from the tables show a reduction in the overall mass loss over the 60 minutes of testing at higher velocities compared to impact velocity of 16.3ms^{-1}.

Preprints (www.preprints.org) | NOT PEER-REVIEWED | Posted: 5 August 2020 doi:10.20944/preprints202008.0098.v2

***Table 5**: Mass loss of steel samples at 16.3ms^{-1} with changing raindrop diameter*

	Mass loss of steel at specified rain drop diameters (mg)		
Time (min)	**2mm**	**2.5mm**	**2.8mm**
0	0	0	0
20	0.4	0.4	0.5
40	0.9	0.7	0.2
60	1.5	1.2	0.7

***Table 6**: Mass loss of steel samples at 32.9ms^{-1} with changing raindrop diameter*

	Mass loss of steel at specified rain drop diameters (mg)		
Time (min)	**2mm**	**2.5mm**	**2.8mm**
0	0	0	0
20	0.6	0.2	0.2
40	0.9	0.3	0
60	0.9	0.9	0.4

***Table 7**: Mass loss of steel samples at 47.7ms^{-1} with changing raindrop diameter*

	Mass loss of steel at specified rain drop diameters (mg)		
Time (min)	**2mm**	**2.5mm**	**2.8mm**
0	0	0	0
20	-0.1	0.8	0.3
40	0.4	1.0	0.8
60	0.5	1.1	0.9

***Table 8**: Mass loss of steel samples at 60.5ms^{-1} with changing raindrop diameter*

Preprints (www.preprints.org) | NOT PEER-REVIEWED | Posted: 5 August 2020 doi:10.20944/preprints202008.0098.v2

	Mass loss of steel at specified rain drop diameters (mg)		
Time (min)	**2mm**	**2.5mm**	**2.8mm**
0	0	0	0
20	0.2	0.3	0.2
40	0.4	0.2	0.5
60	0.5	0.6	1.0

As the velocity is further increased to 47.7ms^{-1} there is still no signs of an increasing mass loss rate (*Table 8*). A transition can be spotted in the results where the larger raindrop diameters produce a greater mass loss at higher velocities in comparison to the lower velocities (*Table 8*).

3.4 SEM images and EDS results

A S3700 (Hitachi, Japan) Tungsten Filament Scanning Electron Microscope (SEM) was used to examine the surface of the mild steel. Initial SEM micrographs prior to impact testing display a flat surface as seen in Figure 4. The black spots seen on the surface of the specimens were found to be impurities of manganese sulphide using energy dispersive spectroscopy (EDS). High levels of oxygen, manganese and sulphur are common in steels, as when the steel is in molten form it is very soluble to oxygen which defuses into the slag (a residue on the surface of the liquid steel) forming the manganese sulphide. These inclusions were considered to have negligible effect on the tests being run in this project but in many cases these inclusions affect the malleability of the steel. Since all test specimens were machined from the same piece of mild steel they were all very similar in comparison to Figure 4.

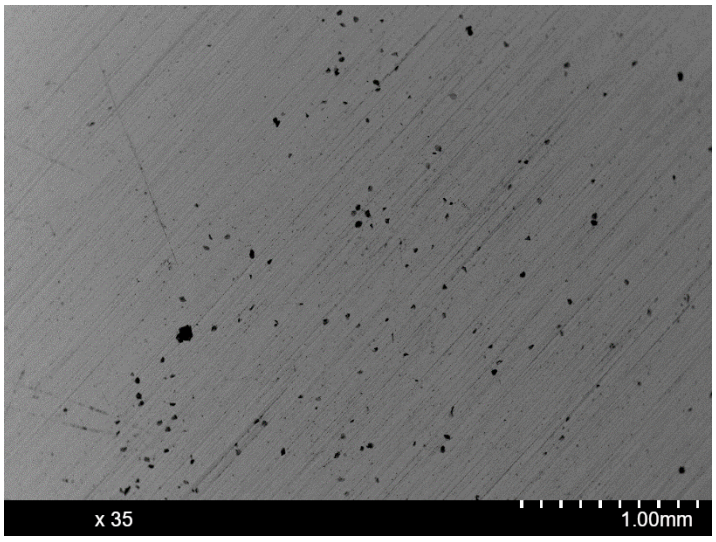

Preprints (www.preprints.org) | NOT PEER-REVIEWED | Posted: 5 August 2020 doi:10.20944/preprints202008.0098.v2

***Figure 4**: Test specimen prior to impact testing*

(*Table 9*) was used to emphasise the composition of elements in the mild steel prior to impact testing. Carbon is ignored from the EDS results as the surface of the specimen is coated with a thin layer of carbon prior to scanning, consequentially the grade of steel is unknown.

***Table 9:** Elements of the mild steel surface prior to impact testing*

Element	**Weight%**
Iron, Fe	99.3
Manganese, Mn	0.7

The micrograph in Figure 5 was taken from a small section of the same sample after 80 minutes of liquid impact testing. Comparison of the two images indicate a change on the surface of the steel due to rain drop impacts. EDS was used to determine the chemical compositions of the testing surface of the mild steel. The results in Table 10 show high oxygen levels, indicating the presence of an iron oxide layer. Elements such as chlorine and sodium may be explained as impurities on the surface of the steel from the tap water used during testing. (It should be noted that Nickel should not be seen on the surface of the mild steel and 10% is an extremely high approximation and was narrowed down to an inaccuracy with the EDS result.)

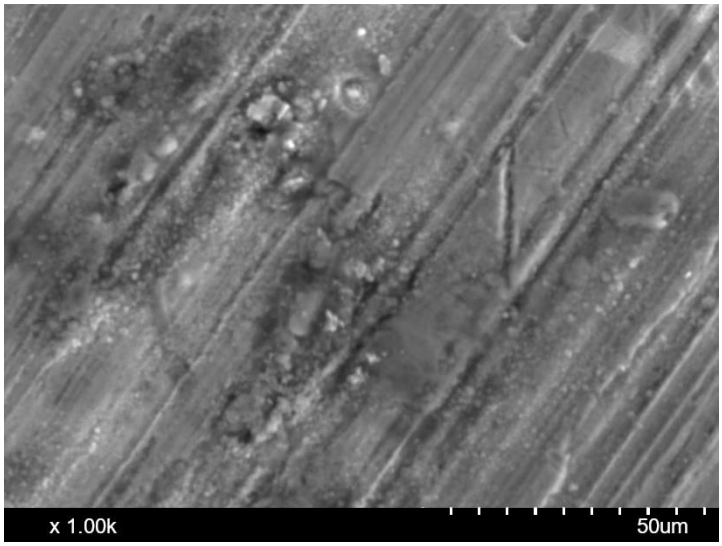

***Figure 5**: Surface of steel sample post impact testing*

***Table 10**: EDS results from the surface of mild steel sample post liquid impact testing*

Element	**Weight%**
Nickel, Ni	10.6

Oxygen, O	21
Sodium, Na	7.5
Chlorine, Cl	4.3
Potassium, K	1.4
Sulphur, S	1.6
Manganese, Mn	0.5
Iron, Fe	53.1

4. Discussion

4.1 RETR validation

The rain erosion test rig (RETR) performed as required and a mass loss of mild steel was recorded. The results acquired in this project found the highest mass loss occurred at 16.3 ms^{-1} of 1.5 mg. Developments proved very successful and the hub now rotates with minimum resonance. The hub and whirling arms are more stable being attached using a keyway joint. A new gear has been attached to the rig producing a gear ratio of 1:2 theoretically doubling the velocity in the range of 120ms^{-1}.

Regardless of low mass losses SEM images and EDS results proved rain drop impacts were occurring at the surface of the steel specimens. The main parameter affecting the accuracy of the result was the updraft due to the rotating arms. With the current design of the (RETR) there is no visual aid proving raindrops are colliding with the surface of the test sample. Confirmation of raindrop impacts at high velocities is therefore a vital next step into the research of rain erosion testing using this rig. The most efficient method would be to apply a stroboscope to the rig.

The new mounts demonstrated a quick and simple method of attaching and removing the test samples. The significant downside to the new mount being the effect of galvanic coupling between the test specimen and the mount. Using a non-corrosive coating on the mounts and the bottom surface of the samples proved successful in stopping these reactions between the surfaces.

Preprints (www.preprints.org) | NOT PEER-REVIEWED | Posted: 5 August 2020 doi:10.20944/preprints202008.0098.v2

4.2 Effects of linear velocity on the erosion of mild steel

The results from (*Table 4*) are presented in (*Figure 6*) below, indicating a mass loss as the velocity is increased from 16.3ms^{-1} to 60.5ms^{-1} over 80 minutes of testing. Two test specimens were tested and the mass loss can be seen to increases almost linearly. Both test specimens have a fluctuation in the mass loss at 20 ms^{-1}. The uncertainty in the results from the weighing scales was found to be roughly $\pm 0.1mg$ indicated by the error bars in Figure 6. It was presumed the mass loss vs velocity graph would indicate an increasing gradient as the impact energy increased exponentially with the rising velocity. An increasing impact energy would suggest more impact damage and a larger mass loss. [13]. Interestingly McGechaen (2013) (14) discovered a similar trend and from Lee (1990)(17), the mass loss measurements of steel are linearly related to the quantity of ferrite in the microstructure, suggesting a tribo-corrosion mechanism in operation. [14]

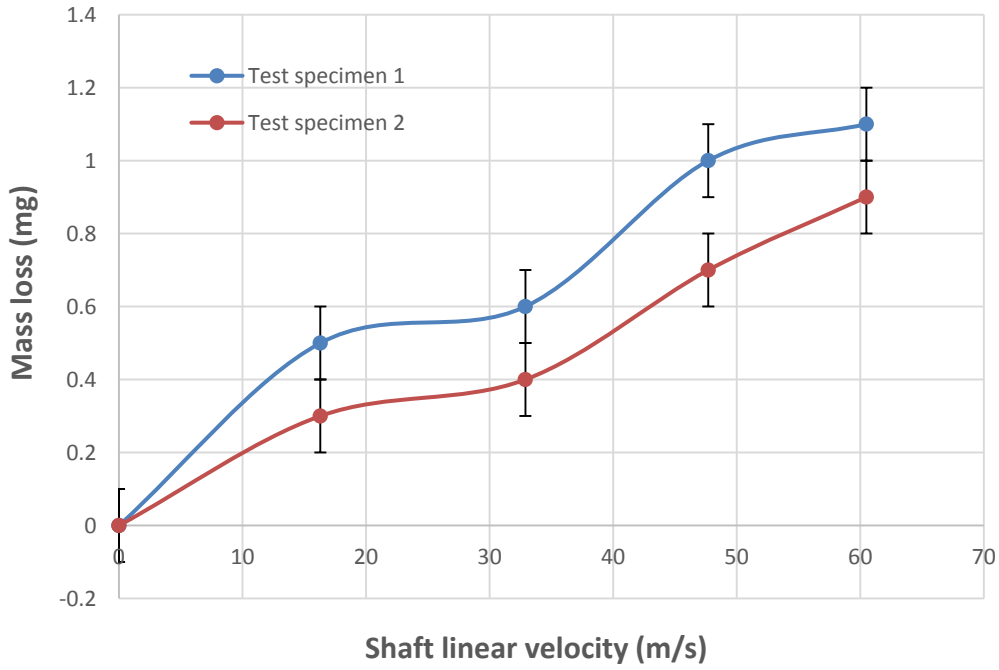

Figure 6: *Cumulative mass loss of steel specimens*

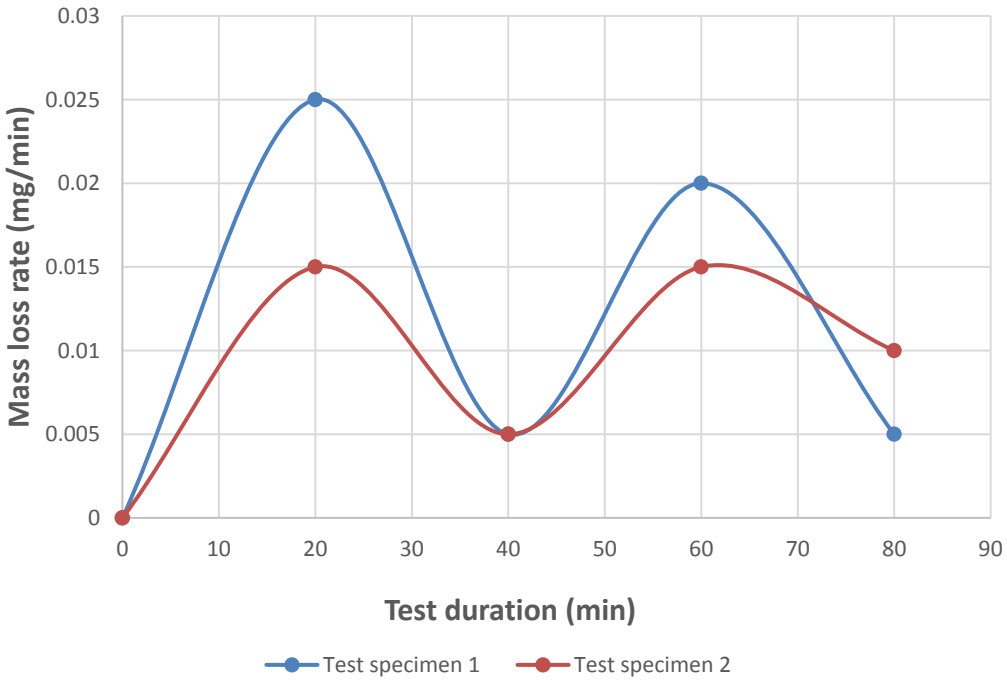

Figure 7: *Mass loss rate of steel specimens*

In an attempt to explain the effect of increasing linear velocity on the mass loss of mild steel the data was normalized to produce a graph of the mass loss rate during the test, represented in Figure 7. Previous work showed a gradual increase in the mass loss rate with rising linear velocity.[14].[G] The graph presented in Figure 7 on the contrary indicates a very different trend, between 20 min and 40 min in that there is a rapid depletion in mass loss rate. Interestingly during testing in previous work a drop in the mass loss rate was found, although slightly later into the test which could be an indication of an incubation period. [15]. Measurements were only taken every 20 minutes and thus it is quite possible that the incubation period was missed. Lee (1990) [15] identified an incubation period of roughly 2 minutes for steel containing 0.41% Carbon. After 40 minutes the mass loss rate starts increasing again signifying erosion of the mild steel as expected after the incubation period, which was proposed by Tobin et al. [12]. Extending the test duration and increasing the number of intervals the specimen is weighed would greatly improve the chances of identifying the incubation period.

Unexpectedly (*Figure 7*) shows another large drop in the mass loss rate 60 minutes into testing. Tobin et al. proposes after the incubation period the wear mechanism tends towards an erosion-corrosion process and the mass loss rate should continue increasing at higher velocities. [16]. During testing, visual observations indicated that at high velocities rain droplets would accumulate on the wall of the container and slowly spiral downwards, suggesting many raindrops may not be colliding with the surface of the test specimen. There is no theoretical evidence to verify this theory as the rig is unable to identify raindrop collisions on the surface of the test specimen. A reduction of impacts would certainly contribute to a reduced mass loss rate at higher velocities.

Preprints (www.preprints.org) | NOT PEER-REVIEWED | Posted: 5 August 2020 doi:10.20944/preprints202008.0098.v2

The following graphs in Figures 8, 9 and 10 represent the total mass at the end of testing for various linear wind velocities, using a constant raindrop diameter. Each test was run for 1 hour and the total mass loss was recorded. All three graphs show signs of the updraft having an effect on the mass loss between 20ms^{-1} - 30ms^{-1} highlighting a similar conclusion that the updraft must be affecting the number of raindrops colliding with the surface. In all three graphs there is a rise in mass loss at higher wind velocities at around 50ms^{-1}, this could be related to the increasing impact energy. Although many rain droplets are not colliding with the surface the few that are will be causing greater damage, leading to the increase in mass loss.

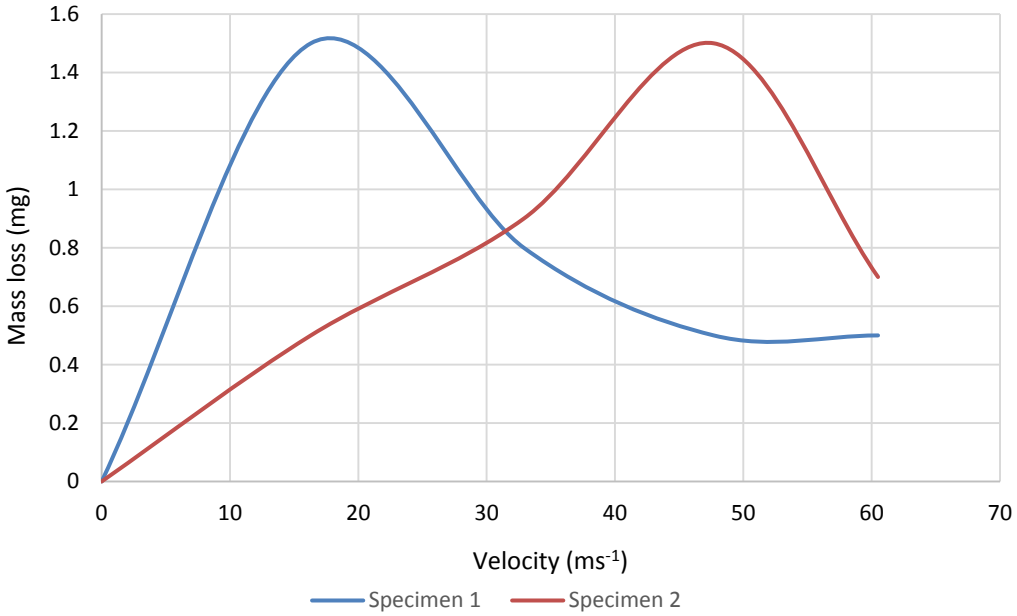

Figure 8: *Mass loss at raindrop diameter 2mm with increasing linear velocity*

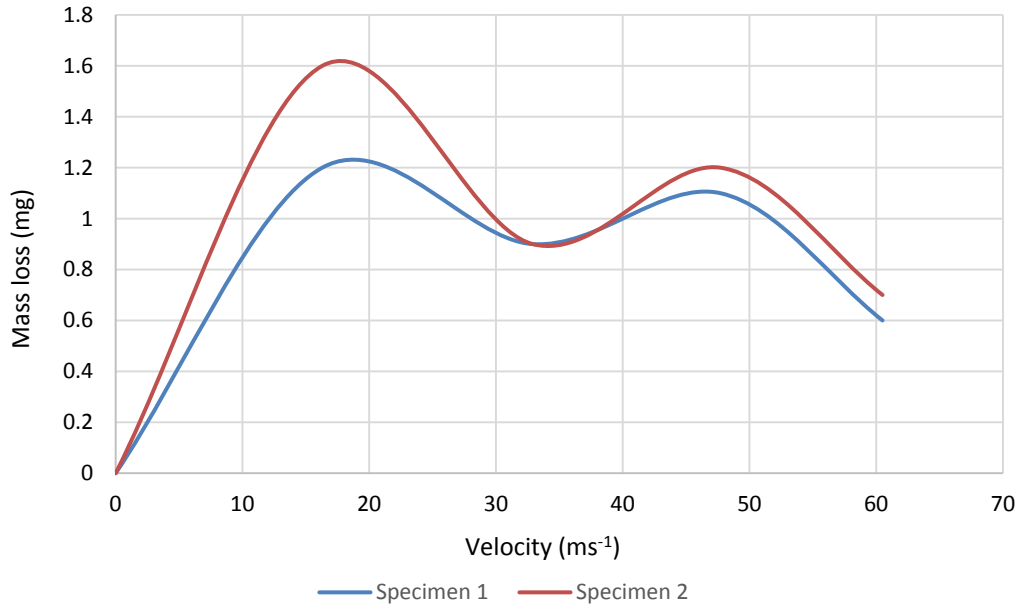

Figure 9: *Mass loss at raindrop diameter 2.5mm with increasing linear velocity*

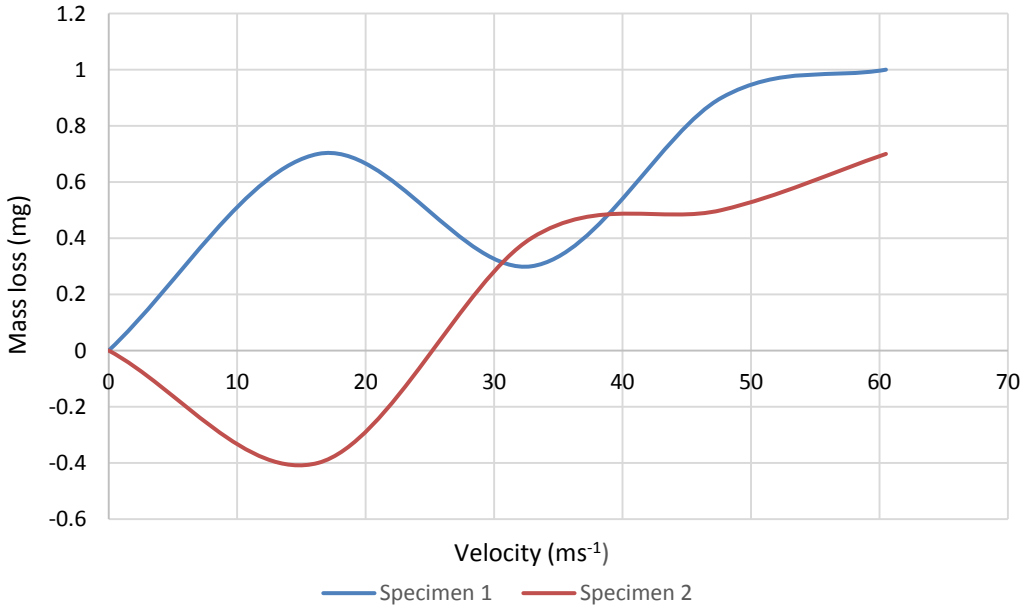

Figure 10: *Mass loss at raindrop diameter 2.8mm with increasing linear velocity*

Preprints (www.preprints.org) | NOT PEER-REVIEWED | Posted: 5 August 2020 doi:10.20944/preprints202008.0098.v2

4.3 Effects of raindrop diameter on the erosion of mild steel

Graphs were created to illustrate the effect of varying raindrop diameters have with increasing linear velocity on the mild steel. Figure 11 shows the effect of varying the raindrop diameter has on the erosion at the surface of mild steel at 16.3ms^{-1}. The interesting observation made from formulating the data in this format is the mass loss at velocity 16.3ms^{-1}, clearly shows a decreasing mass loss with increasing rain drop diameter. This was not expected as obviously with increasing diameter the surface area of the rain droplet colliding with the sample is larger, leading to a greater water hammer pressure.

Rain droplet diameters 2.0mm and 2.5mm can be seen to have a gradual mass loss with evidence of an increasing mass loss rate near 60 minutes. The 2.8mm diameter however has an increase in mass at 20 minutes; this could be a sign of the incubation period where an iron oxide layer is forming, acting initially as a protective coating against erosion as has been indicated for elevated temperature erosion. [19, 21]

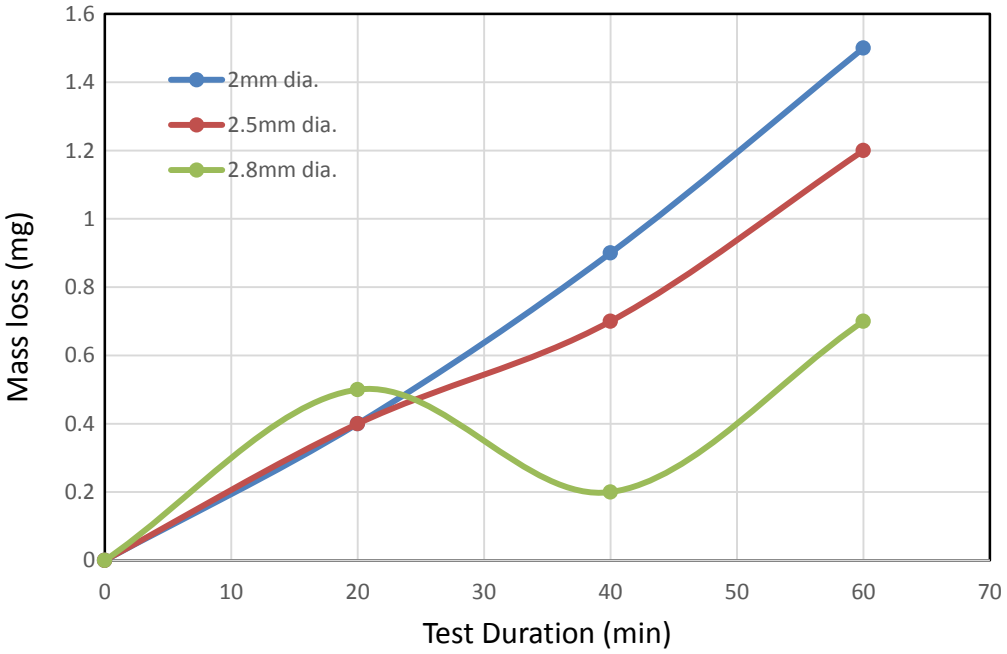

Figure 11: *Total mass loss of steel at 16.3ms^{-1} with varying rain drop diameter*

Referring to (*Figure 11*) the 2mm raindrop diameter provides the greatest damage due to erosion. Possible reasons for this could be that at lower velocities, the updraft is too low to disrupt the trajectory of any raindrop diameter size and with a constant flow rate the smaller gauged needles will produce more rain drops per minute. Perhaps leading to additional impacts on the surface of the specimen, this further bombardment of raindrops will give less time for the surface to cool down leading to greater erosion-corrosion. Other work states that the increase in temperature causes a

Preprints (www.preprints.org) | NOT PEER-REVIEWED | Posted: 5 August 2020 doi:10.20944/preprints202008.0098.v2

decrease in fluid viscosity resulting in a larger Reynolds number, consequently increasing the erosion. [19]The temperature on the surface of the material will also have detrimental effect on the material properties of the mild steel such as yield stress, subsequently reducing mechanical resistance. Figure 12 illustrates a very similar trend where the 2.0mm diameter raindrops produce the greatest mass loss. However after 40 minutes the mass loss rate of the 2mm diameter rain droplets level off, whereas the 2.5mm and 2.8mm diameters can be seen to increase significantly. Continuing rain drop impact testing after the 40 minute period or incubation period showed rise to greater mass loss rates, as erosion of the iron oxide layer exposes more of the mild steel.

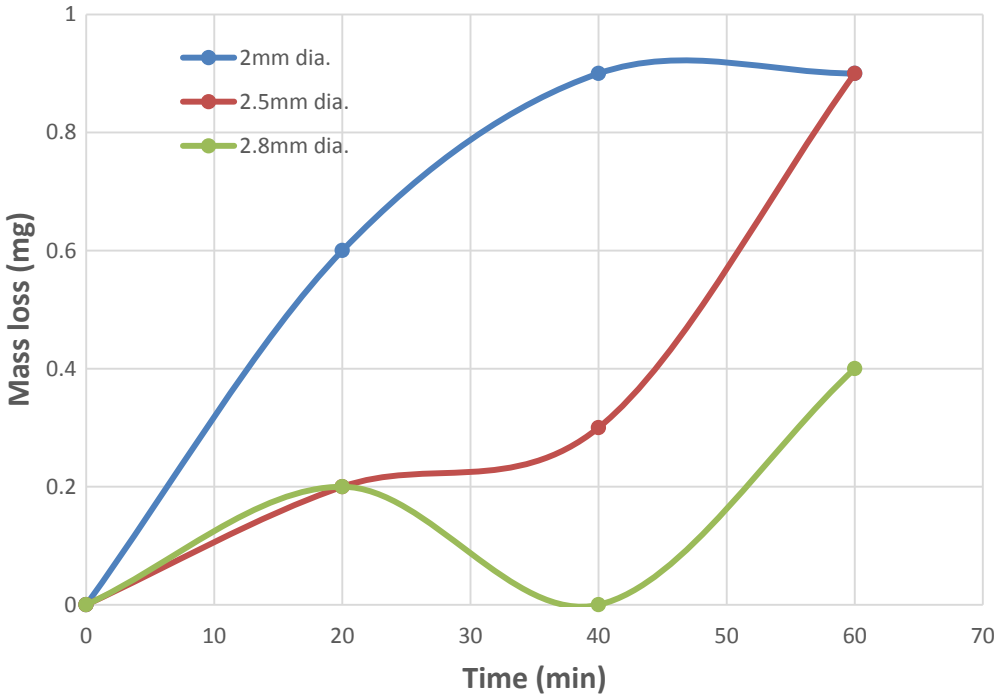

Figure 12: *Total mass loss of steel at 32.9ms^{-1} with varying rain drop diameter*

As the velocity further increases there appears to be a transition phase where the larger raindrop diameters start producing greater mass loss, which is demonstrated in Figures 13 and 14. A theory was that the larger rain droplets are heavier in mass resulting in the updraft having less effect compared to the smaller raindrop diameters. For future research it could be considered to take the mass loss measurements after 5 minute periods and to increase the test duration, which in theory would improve the accuracy of the graphs and would help determine a more realistic incubation period.

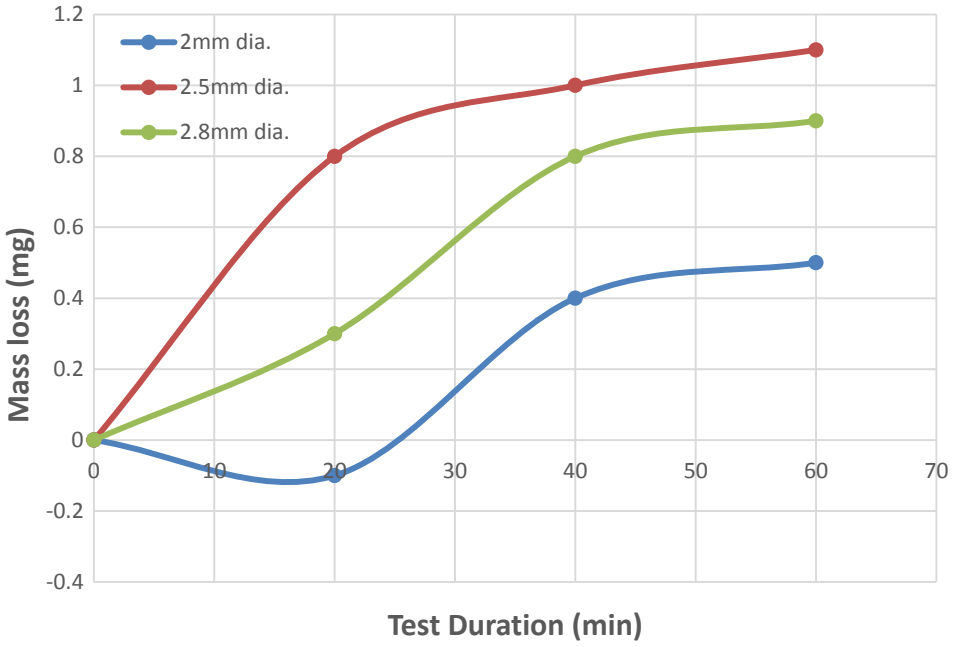

Figure 13: *Total mass loss of steel at 47.7ms^{-1} with varying rain drop diameter*

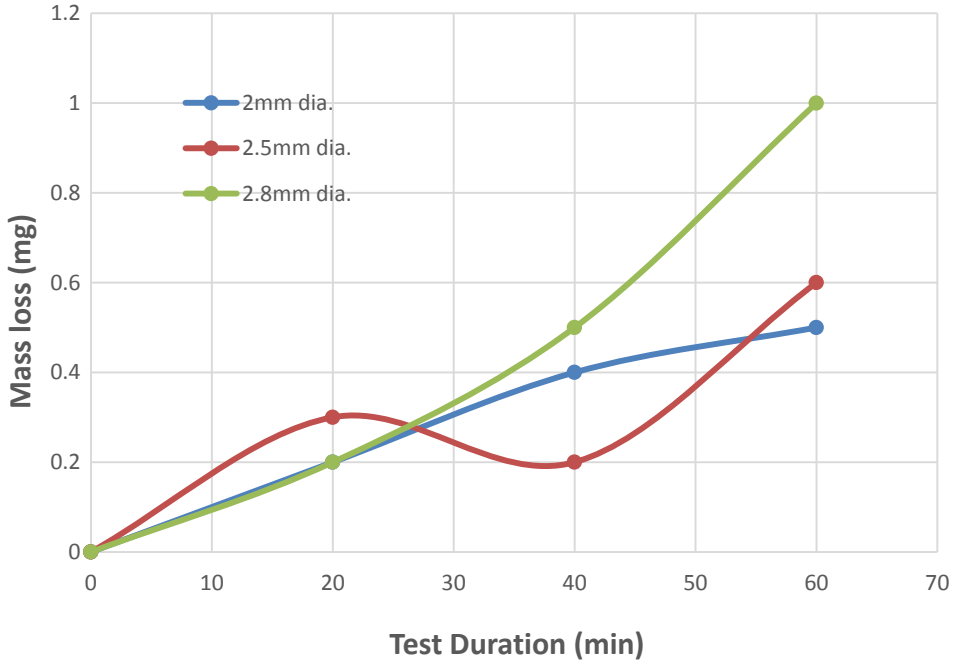

Figure 14: *Total mass loss of steel at 60.5ms^{-1} with varying rain drop diameter*

Figures 11, 12, 13 and 14 confirm an erosion-corrosion process is occurring. Previous work by Stack illustrates that erosion and corrosion are two competing processes that can occur simultaneously on the mild steel surface. [19, 23]. During an erosion-corrosion process formation of a passive film acts

Preprints (www.preprints.org) | NOT PEER-REVIEWED | Posted: 5 August 2020 doi:10.20944/preprints202008.0098.v2

as a barrier between the mild steel surface and the action of the raindrop impacts causes the oxidation rate of iron to slow down while the scale thickens.[16, 19]

4.4 SEM and EDS post rain drop impact testing

From section 4.2, there were clear signs of erosion taking place on the surface of the test specimens due to raindrop impacts. Images were taken with a camera to give a clearer representation of the whole test specimen compared to SEM micrographs, allowing the oxide layer to be seen more clearly.

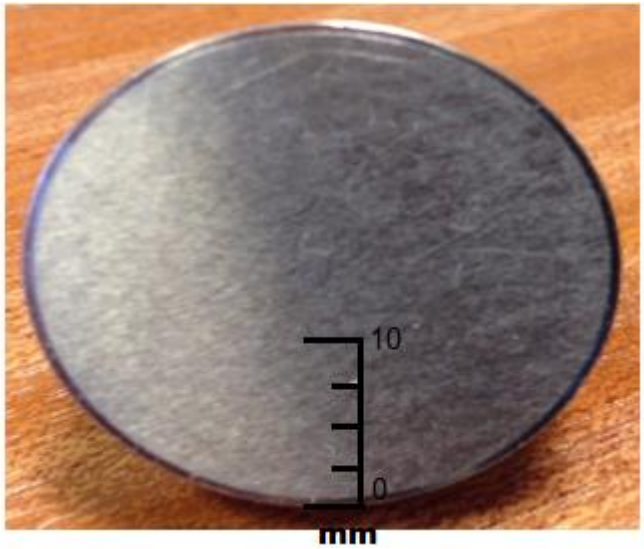

***Figure 15**: Steel sample prior to impact testing*

Preprints (www.preprints.org) | NOT PEER-REVIEWED | Posted: 5 August 2020 doi:10.20944/preprints202008.0098.v2

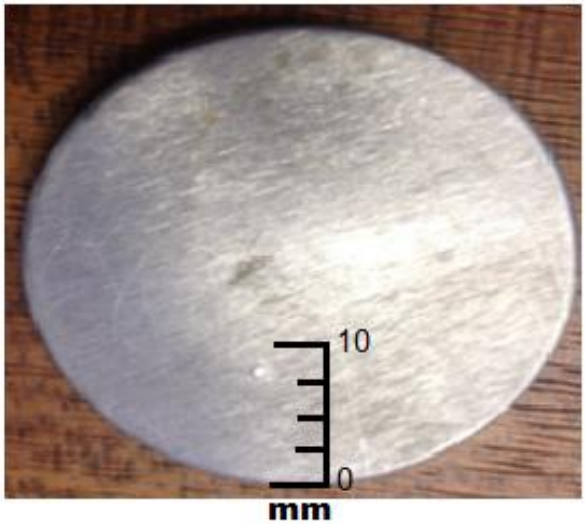

Figure 16: **A)** *Test sample at 16.3ms^{-1}*

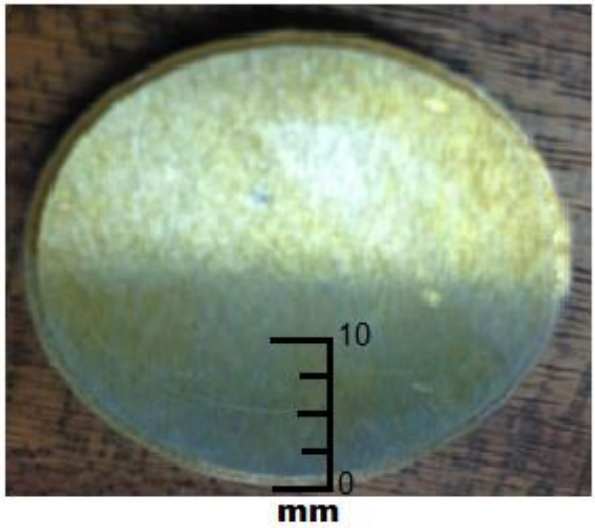

B) *Test sample at 32.9ms^{-1}*

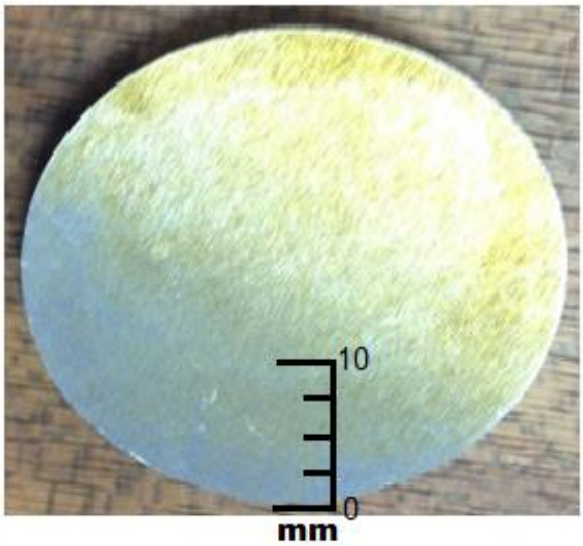

C) *Test sample at 47.7ms^{-1}*

D) *Test sample at 60.5ms^{-1}*

Comparing the images after liquid impact testing of various linear velocities at a constant raindrop diameter of 2mm (*Figure 16*), to the image of the samples prior to testing seen in Figure 15, clear evidence of an oxide l is visible The main area affected by the rain drop impacts is evident at the top half of the sample where oxide scale has initially formed before spreading across the remaining surface. This observation is in agreement with previous work on rain drop liquid impact testing.

Visually from Figure 16[A] there is very little sign of erosion or corrosion occurring on the sample at the macro scale . The mass loss results however show the greatest mass loss coming from this sample at a velocity of 16.3ms^{-1}. Figure 16[B] shows the iron oxide layer being removed by erosion at 32.9ms^{-1} when comparing to Figure 16[C] testing at 47.7ms^{-1} . The iron oxide layer is much more visible indicating less erosion of the iron oxide scale. Evidence of this can be seen in (*Figure 12*) where the mass loss rate for testing at 32.9ms^{-1} ; this levels off after the 20 minute period however does not yet increase after 60 minutes of testing indicating the oxide layer has not been completely eroded. The 47.7ms^{-1} test shows an increase in the mass loss rate after 20 minutes of impact testing indicating the end of the incubation period (*Figure 13*).

Preprints (www.preprints.org) | NOT PEER-REVIEWED | Posted: 5 August 2020 doi:10.20944/preprints202008.0098.v2

SEM micrographs in Figure 17 shows the surface of the oxidised mild steel after liquid impact testing. Several sites of interest have been numbered in the image and (EDS) analysis was run to observe the conditions on the surface at these specific locations. By comparing the results from (*Table 9*) and (*Table 11*) it can be seen that a high percentage of oxygen is established on the surface after impact testing; however no oxygen was present prior to testing. It is possible that the frictional heating heat produced from rotational process of the raindrop impact and the wet conditions provided an optimal environment for corrosion to occur. Corrosion was seen observed from images in Figure 16.

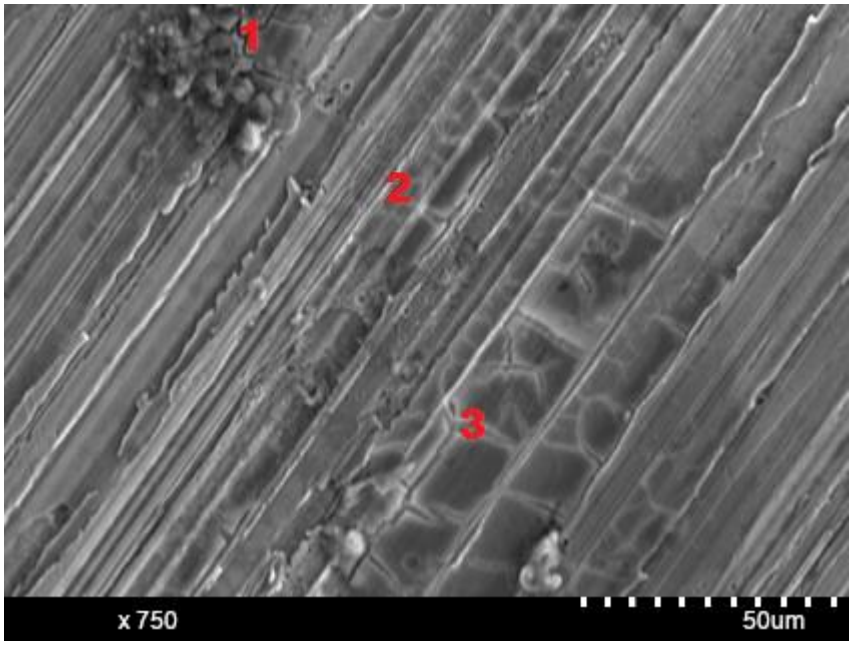

***Figure 17**: SEM micrograph of oxidised steel*

***Table 11**: Elemental analysis for site 1*

Element	Weight%
Oxygen, O	26.9
Sodium, Na	0.89
Chlorine, Cl	7.21
Potassium, K	0.56
Sulphur, S	0.31
Manganese, Mn	0.54
Iron, Fe	63.59

The elemental analysis demonstrates the spread of the scale with each site 1, 2 and 3 having variations of oxygen and iron percentages. From Figure 17 site 1 can be seen to be a lot rougher than sites 2 and 3 indicating that corrosion is further developed in this location. Many elements such as potassium, chlorine, copper and sodium are deposited on the surface of the mild steel from the water during testing.

***Table 12**: Elemental analysis for site 2*

Element	Weight%
Oxygen, O	5.13
Sodium, Na	0.74
Copper, Cu	0.69
Potassium, K	0.56
Sulphur, S	0.27
Manganese, Mn	2.41
Iron, Fe	88.90

***Table 13**: Elemental analysis for site 3*

Element	Weight%
Oxygen, O	2.46
Sodium, Na	0.49
Potassium, K	0.18
Manganese, Mn	0.59
Iron, Fe	96.28

Site 3 indicates a low oxygen level of 2.46% (*Table 13*) which indicates the scale of the passive film has not developed as much as site 1 which has an oxygen level of 26.9% (*Table 11*). From the micrograph formations of stress cracks can be seen at site 3. This could be an indication of an erosion-corrosion dominant phase where the passive film is being eroded by the liquid impacts. Previous work indicates that erosion begins to enhance corrosion through the removal of an iron oxide layer, as the temperature will increase with repetitive impacts on the surface enhancing the corrosion. [20] Removal of oxide scale thus becomes the main mass loss mechanism.[14]

Preprints (www.preprints.org) | NOT PEER-REVIEWED | Posted: 5 August 2020 doi:10.20944/preprints202008.0098.v2

4.5 Raindrop Erosion maps

Wastage maps are very important to the tribology field and are used to estimate the magnitude of material loss. These maps show the material loss (mg) considered whether the wastage is low, medium or high. A wastage map was created using the mass losses recorded during testing with respect to varying rain droplet diameter and linear velocity. Previous research on wastage maps for whirling arm rain erosion rigs from the group have addressed this issue, [20–24]. Initial parameters for low, medium and high mass loss had to be chosen. Mass loss ranges are as follows;

Low [<1 (mg)], Medium [1 - 2.5 (mg)] and High [>2.5 (mg)]

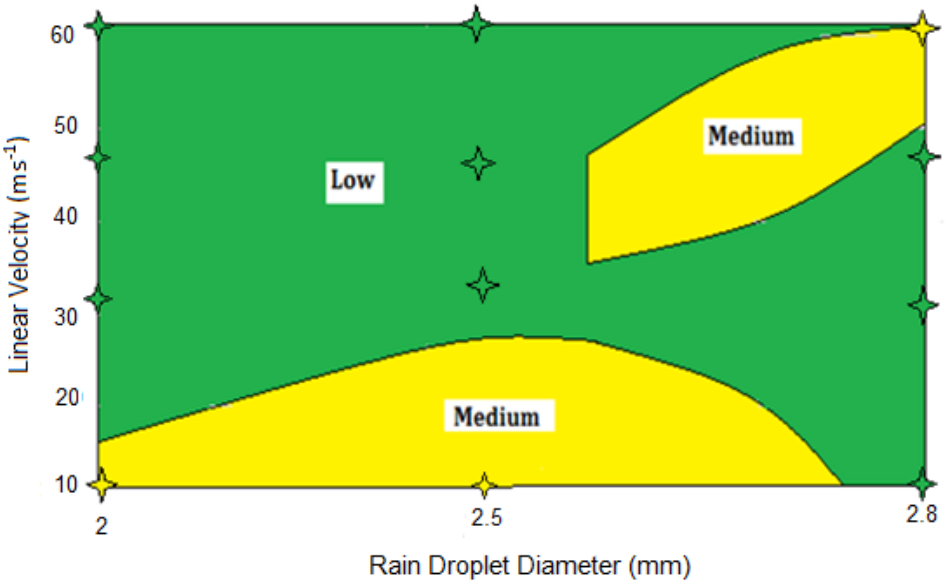

***Figure 18**: Wastage map for mild steel*

The highest mass loss regions were of medium erosion symbolised in (*yellow*) in Figure 18 above. The largest region of medium mass loss was found at lower velocity between 16.3ms^{-1} and 20ms^{-1} which was unexpected. The higher mass loss was expected from larger wind velocities. The second medium region can be seen in the top right hand corner of the wastage map. This section is more expected of a wastage map for a whirling arm rain erosion test rig as the increasing rain droplet diameter and velocity increases the impact energy on the surface which accelerates erosion. No high mass loss was found during any of the tests on (RETR, the main reason being the linear velocities are very low in comparison to work done by other researchers. The transition to low wastage at higher velocities at the lower right hand corner of the map is possibly indicative of transitions to oxide formation due the frictional heating process as discussed above and or effects of jetting, as discussed below.

Preprints (www.preprints.org) | NOT PEER-REVIEWED | Posted: 5 August 2020 doi:10.20944/preprints202008.0098.v2

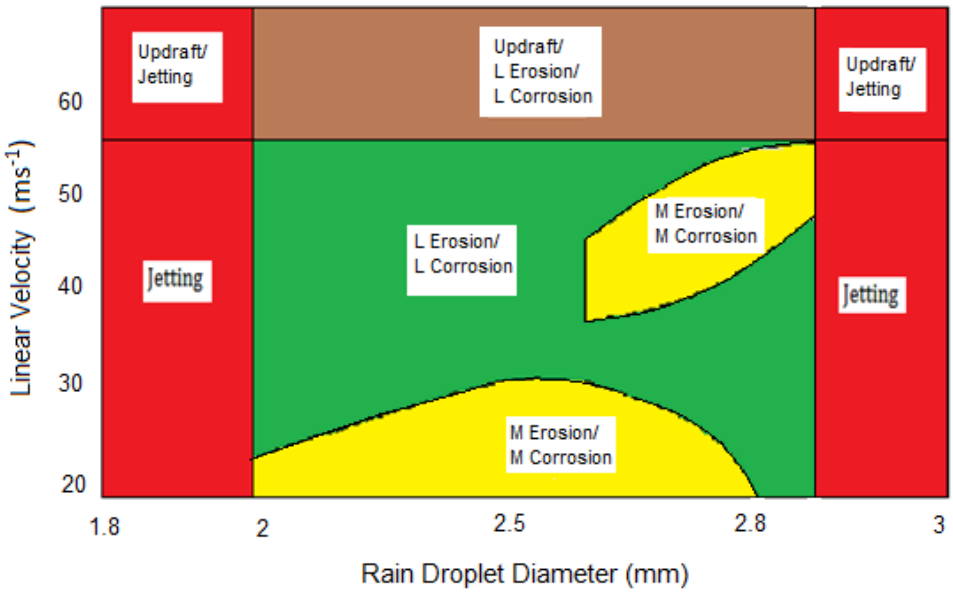

***Figure 19**: Wastage map showing various raindrop processes at given test conditions*

During testing of raindrop diameters 1.8mm, formation of jets were occurring instead of rain droplets from the ends of the needles. An attempt to produce rain droplets of 1.8mm diameter was done by reducing the flow rate to 10 mL/min, less than half of the required volume flow rate. A reduction in pressure could still not produce rain droplets, so tests had to be voided. A similar problem arose from needles producing 3.0mm diameter raindrops, where the formation of water jets would occur from a couple of the needles. Figure 19 is used to illustrate the transition of rain droplet effects encountered during testing caused by jetting from the needles and updraft from the whirling arms. L and M symbolises Low erosion/ corrosion and Medium erosion/ corrosion respectively.

Preprints (www.preprints.org) | NOT PEER-REVIEWED | Posted: 5 August 2020 doi:10.20944/preprints202008.0098.v2

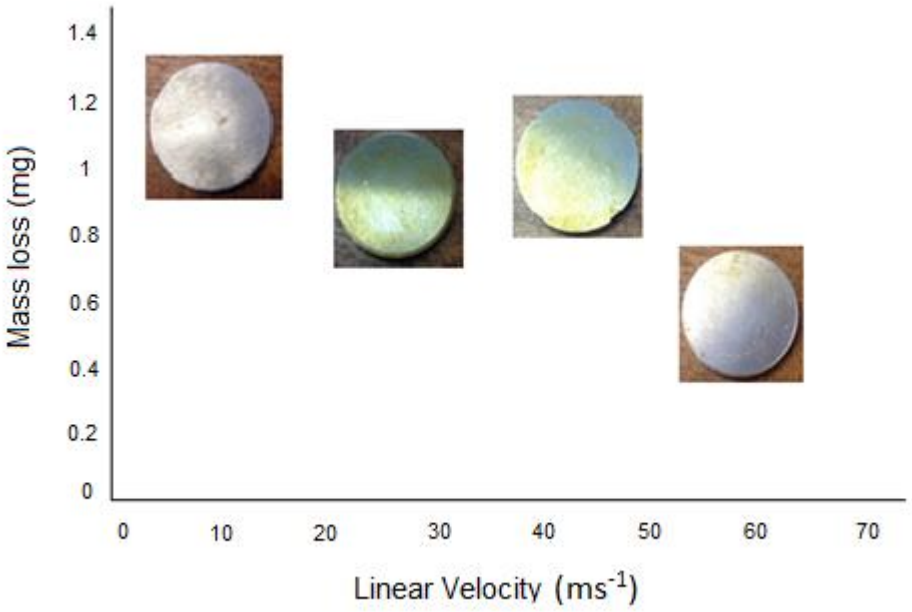

Figure 20: Mass loss graph visualising the effects of corrosion

A further visualization map of the surfaces was produced to compare with the above wastage maps. The graph below (*Figure 20*) was created to illustrate morphological changes on the surfaces of the specimen. Clearly the surface appearances of corrosion product correspond to areas of higher wastage, *Figures. 18 &19* above.

Hence, the maps indicate that these are potentially useful tools for assessing raindrop erosion mechanisms. The interactions between erosion and corrosion can be identified on the maps and/or the increase in frictional heating of the steel surfaces at the higher velocities. Regions where aerodynamic effects are observed are also identified on the maps. Further work will be to assess in more detail the change in oxide composition over a higher velocity range for this material.

5. Conclusions

1) SEM and EDS provide substantial evidence of erosion and the formation of an iron oxide layer signifying an erosion-corrosion process during raindrop erosion of steel.

2) The results indicate that updraft affects the intensity of raindrops colliding with the test specimen surface

3) Erosion wastage maps were created for varying rain droplet diameter and linear wind velocity showing the conditions where raindrop erosion was affected by corrosion and the window of conditions where aerodynamic effects reduced the efficiency of the collisions.

1. Department of Trade and Industry (2003) Our energy future - creating a low carbon economy. London

2. Webster R (2013) UK energy statistics show wind power and biomass push renewable electricity to record high - for a bit | Carbon Brief. In: carbonbrief. https://www.carbonbrief.org/uk-energy-statistics-show-wind-power-and-biomass-push-renewable-electricity-to-record-high-for-a-bit. Accessed 3 Aug 2020

3. EWEA (2011) Design limits and solutions for very large wind turbines . Brussels

4. Field JE (1999) ELSI conference: invited lecture: Liquid impact: theory, experiment, applications. Wear 233–235:1–12. https://doi.org/https://doi.org/10.1016/S0043-1648(99)00189-1

5. Keegan MH, Nash DH, Stack MM (2013) On erosion issues associated with the leading edge of wind turbine blades. J Phys D Appl Phys 46:383001. https://doi.org/10.1088/0022-3727/46/38/383001

6. Hutchings IM (1992) Ductile-brittle transitions and wear maps for the erosion and abrasion of brittle materials. J Phys D Appl Phys 25:A212--A221. https://doi.org/10.1088/0022-3727/25/1a/033

7. Hattori S, Takinami M (2010) Comparison of cavitation erosion rate with liquid impingement erosion rate. Wear 269:310–316. https://doi.org/https://doi.org/10.1016/j.wear.2010.04.020

8. Wood K (2011) Blade repair: Closing the maintenance gap. In: CompositesWorld. https://www.compositesworld.com/articles/blade-repair-closing-the-maintenance-gap. Accessed 3 Aug 2020

9. 3M Wind Energy Solutions. In: 3M. https://www.3m.com/3M/en_US/power-generation-us/solutions/wind-energy/. Accessed 3 Aug 2020

10. Kubilay A, Derome D, Blocken B, Carmeliet J (2013) CFD simulation and validation of wind-driven rain on a building facade with an Eulerian multiphase model. Build Environ 61:69–81. https://doi.org/https://doi.org/10.1016/j.buildenv.2012.12.005

11. Best AC (1950) The size distribution of raindrops. Q J R Meteorol Soc 76:16–36. https://doi.org/10.1002/qj.49707632704

12. Tobin EF, Young TM, Raps D, Rohr O (2011) Comparison of liquid impingement results from whirling arm and water-jet rain erosion test facilities. Wear 271:2625–2631. https://doi.org/https://doi.org/10.1016/j.wear.2011.02.023

13. Stack MM, Abdulrahman GH (2010) Mapping erosion-corrosion of carbon steel in oil exploration conditions: Some new approaches to characterizing mechanisms and synergies. Tribol Int 43:1268–1277. https://doi.org/10.1016/j.triboint.2010.01.005

14. R. McGechaen. (2013) MEng (University of Strathclyde

15 . N. Krishnamurthy, M.S. Murali, B.Venkataraman and P.G. Mukunda (2012) Erosion behaviour of plasma sprayed alumina and Calcia-Stabilized Zirconia coatings on cast iron substrate,

ceramic coatings – Applications in Engineering, Prof. Freg Shi (ED.), ISBN: 978-953-0083-6, InTech,.

Available at: http://www.intechopen.com/books/ceramic-coatings-applications-in-engineering

16. G.M.C. Lee (1990) The erosion resistance of plain steels under water droplet impacts conditions. Wear. 141 pp. 185-201

17. E.F. Tobin, T.M. Young, D. Raps,. (2012) Evaluation and correlation laboratory results from a rain erosion test campaign. 28th International congress of the aeronautical sciences.

Available at: http://www.icas.org

18 . Finnie I. (1972) Some observations on the erosion of ductile materials: Wear, 19 (1972) 81-90.

19. Stack MM, Stott FH, Wood GC (1993) Review of mechanisms temperatures of erosion-corrosion of alloys at elevated. Wear 162–164:706–712

20. Stack MM, Abdelrahman SM, Jana BD (2010) Some perspectives on modelling the effect of temperature on the erosion–corrosion of Fe in aqueous conditions. Tribol Int 43:2279–2297. https://doi.org/https://doi.org/10.1016/j.triboint.2010.07.015

21. Stack MM, Stott FH, Wood GC (1992) The effect of pre-oxidation of chromia and alumina forming alloys on erosion in laboratory simulated fluidized-bed conditions. Corros Sci 33:965–983. https://doi.org/https://doi.org/10.1016/0010-938X(92)90059-C

22. Rasool G, Middleton AC, Stack MM (2020) Mapping Raindrop Erosion of GFRP Composite Wind Turbine Blade Materials: Perspectives on Degradation Effects in Offshore and Acid Rain Environmental Conditions. J Tribol 142:. https://doi.org/10.1115/1.4046014

23. Pugh K, Rasool G, Stack MM (2019) Raindrop Erosion of Composite Materials: Some Views on the Effect of Bending Stress on Erosion Mechanisms. J Bio- Tribo-Corrosion 5:45. https://doi.org/10.1007/s40735-019-0234-8

24. Pugh K, Rasool G, Stack MM (2018) Some Thoughts on Mapping Tribological Issues of Wind Turbine Blades Due to Effects of Onshore and Offshore Raindrop Erosion. J. Bio- Tribo-Corrosion 4:50

Preprints (www.preprints.org) | NOT PEER-REVIEWED | Posted: 5 August 2020 doi:10.20944/preprints202008.0098.v2

References